Noncollective aligned and antialigned states in ^{125}I

Purnima Singh, Somnath Nag, and A. K. Singh
Department of Physics & Meteorology, Indian Institute of Technology Kharagpur, IN-721302, India

H. Hübel, A. Al-Khatib, P. Bringel, C. Engelhardt, and A. Neußer-Neffgen
Helmholtz-Institut für Strahlen- und Kernphysik, Universität Bonn, Nussallee 14-16, D-53115 Bonn, Germany

I. Ragnarsson
Department of Mathematical Physics, Lund Institute of Technology, Box 118, S-221 Lund, Sweden

M. P. Carpenter, R. V. F. Janssens, T. L. Khoo, and T. Lauritsen
Argonne National Laboratory, Argonne, Illinois 60439, USA

G. B. Hagemann, C. R. Hansen, B. Herskind, and G. Sletten
Niels Bohr Institute, Blegdamsvej 17, DK-2100 Copenhagen Ø, Denmark

A. Bracco, G. Benzoni, and F. Camera
Dipartimento di Fisica, Universit'a di Milano and INFN, I-20133 Milano, Italy

P. Fallon and R. M. Clark
Nuclear Science Division, Lawrence Berkeley National Laboratory, Berkeley, California 94720, USA

P. Chowdhury
University of Massachusetts Lowell, Lowell, Massachusetts 01854, USA

H. Amro
Department of Physics, Mississippi State University, Mississippi 39762, USA
(Received 7 January 2010; revised manuscript received 13 July 2010; published 1 September 2010)

High-spin states in ^{125}I were populated using the reaction ^{82}Se(^{48}Ca, $p4n$) at a beam energy of 200 MeV and γ-ray coincidence events were acquired with the Gammasphere spectrometer. The level scheme of ^{125}I was extended considerably. In particular, maximally aligned states involving all eleven particles outside the ^{114}Sn core were observed. Comparison with cranked Nilsson-Strutinsky calculations suggests that three of these states are the final I_{max} states in terminating bands with all spin vectors aligned along a common axis. In two of these, one spin vector is antialigned and points in the opposite direction. In one of the states two spin vectors are antialigned. This is the first observation of a state with such a structure.

DOI: 10.1103/PhysRevC.82.034301 PACS number(s): 21.10.Re, 23.20.En, 23.20.Lv, 27.60.+j

I. INTRODUCTION

The nuclei near the closed shell at $Z = 50$ with mass number $A \simeq 125$ show a rich variety of structure effects associated with significant variations of shape and deformation. They are soft with respect to triaxiality and the strong deformation-driving forces of high-j proton and neutron orbitals stabilize the prolate and oblate deformation, respectively. This behavior is characteristic for the I isotopes ($Z = 53$), which lie in the transitional region between the near-spherical Sn ($Z = 50$) and the deformed Ce ($Z = 58$) nuclei. Well-developed rotational structures, built on proton $h_{11/2}$ states, occur in the light odd-mass I nuclei ($A < 121$) [1]. In contrast, negative-parity states in the heavier odd-mass I isotopes ($A > 121$), associated with the neutron $h_{11/2}$ orbital, show a vibrational structure similar to the neighboring even-mass Te isotopes [2].

Intruder bands, extending to very high spin and excitation energy, have been observed in the light odd-A isotopes $^{113-117}$I. They are believed to involve two-particle–two-hole (2p-2h) excitations across the $Z = 50$ shell gap from the $g_{9/2}$ orbital. These bands exhibit the unique feature of smooth band termination [3–6], where the nucleus traces, over many transitions, a gradual path through the γ plane from a collective prolate to a noncollective oblate shape [7]. During this gradual shape transition, the single-particle angular momenta of the valence nucleons outside the core are gradually aligned toward the rotational axis. However, smooth band termination has not been observed in heavier I isotopes.

Furthermore, in recent spectroscopic studies of the nuclei near $N = 70$, ^{126}Xe [8] and ^{124}Ba [9], several highly deformed bands with remarkable regularity extending to very high spins were discovered. It was suggested that these bands involve deformation-driving neutron $i_{13/2}$ and, possibly, $j_{15/2}$ intruder orbitals.

By considering only the orbitals above the ^{114}Sn core, the maximum angular momentum available within this valence space is limited and lies fully within reach of presently available γ-ray spectrometers. Therefore, these nuclei are well suited for a detailed study of the transition from collective to noncollective excitations and allow the investigation of the properties of and the interplay between configurations with low or no collectivity.

The neutron orbitals available in the nuclei above the ^{114}Sn ($Z = 50$, $N = 64$) core are identical to the proton orbitals for the nuclei above the ^{146}Gd ($Z = 64$, $N = 82$) core. Furthermore, protons and neutrons are distributed over the valence shells in a similar way in the two regions [10,11]. This is interesting because, in the $A = 155$–160 region, terminating bands were observed for the first time; see Ref. [10] for an early review. New features of the interplay between single-particle and collective degrees of freedom have recently been explored (see, e.g., Refs. [12,13]).

Maximally aligned states, where the spin vectors of all valence nucleons outside the ^{114}Sn core are aligned, are of special interest. Such states have been observed at $I^\pi = 55/2^-$ in ^{121}I [14] with seven valence particles, at $I^\pi = 63/2^-$ and $67/2^+$ in ^{123}Cs [11] with nine valence particles, and at $I^\pi = 34^+$ in ^{124}Xe [15] with ten valence particles. The coupling scheme of the valence particles is rather simple: for example, $\pi[(h_{11/2})^1_{11/2}(g_{7/2}d_{5/2})^2_6]_{23/2} \otimes \nu[(h_{11/2})^4]_{16^+}$ for ^{121}I and $\pi[(h_{11/2})^2_{10}(g_{7/2}d_{5/2})^2_6]_{16} \otimes \nu[(h_{11/2})^6]_{18^+}$ for ^{124}Xe, where the superscripts indicate the number of particles involved and the subscripts the maximum spin. Fully aligned states have tentatively been reported also at $I^\pi = 47/2^-$ in ^{121}Te [16], at $I^\pi = 32^+$ in ^{122}Xe [17], and at $I^\pi = 36^+$ in ^{124}Ba [9].

In addition to the noncollective fully aligned states, noncollective states with one or more antialigned particles can be considered. The spin vectors of these particles are also quantized along the rotation axis; however, they point in the opposite direction. Only a limited number of such states has been identified thus far. The first state with such a structure was observed in the $A = 155$–160 region in ^{158}Er (i.e., the $I^\pi = 40^+$ yrast state [18], which has one negative-parity neutron antialigned relative to the $I^\pi = 46^+$ terminating state). Similar states were identified in ^{158,157}Er [18,19] and, somewhat more tentatively, in ^{156}Er [20], where a state with one antialigned $h_{11/2}$ proton was suggested as well. In the region under study here, the only state with such a structure observed thus far is the $I = 39/2$ level [14] in ^{121}I. It has one antialigned $h_{11/2}$ neutron in the configuration of the $I^\pi = 55/2^-$ state specified above. The coupling scheme of these states is rather simple. However, it is surprising that they appear so clearly in experiment, given that many states with the same spin can be formed in other ways.

Prior to this work, low-spin states in ^{125}I were established from β-decay studies of ^{125}Xe [21,22]. Later, high-spin states up to $25/2^+$ and $43/2^-$, respectively, were identified through in-beam spectroscopy [23–28] using small detector arrays. Here, we report on results of an in-beam study of high-spin states in ^{125}I with the aim to search for maximally aligned and antialigned states in this nucleus. Apart from the valence-space configurations, a highly deformed rotational band with characteristics similar to those of one of the highly deformed bands in ^{126}Xe [8] has been observed up to spin $95/2$ and an excitation energy of almost 27 MeV. This band is the subject of a forthcoming publication [29].

In the following, we report mainly on valence-space configurations leading to maximally aligned and antialigned states in ^{125}I. With eleven particles outside the ^{114}Sn core, ^{125}I is the heaviest nucleus where such states have now been observed in this region. Furthermore, comparisons with cranked Nilsson-Strutinsky (CNS) calculations indicate that all the states with aligned and antialigned particles predicted to occur at low energy are observed experimentally. Specifically, to the best of our knowledge, a noncollective state with two antialigned particles has been identified for the first time.

II. EXPERIMENTAL DETAILS AND DATA ANALYSIS

High-spin states in ^{125}I were studied using the heavy-ion fusion evaporation reaction ^{82}Se(^{48}Ca, $p4n$)^{125}I. The ^{48}Ca beam, with an energy of 205 MeV and an intensity of 4 pnA, was provided by the ATLAS accelerator at Argonne National Laboratory. The target consisted of a 0.5 mg/cm^2, 98.8% enriched ^{82}Se layer evaporated on a 0.5 mg/cm^2 Au backing. The Se was protected by a 0.08 mg/cm^2 Au layer. The Au backing faced the beam and, hence, the beam energy at mid-target was about 200 MeV. The beam was slighlty defocused and wobbled over the target, which was mounted on four quadrants of a rotating wheel for heat dissipation on the target foil. Gamma-ray coincidence events were measured with the Gammasphere spectrometer [30]. It consisted of 100 Compton-suppressed Ge detectors at the time of the experiment. In a beam time of seven days, 2.8×10^9 events, with a Ge detector coincidence fold of $f \geqslant 5$, were collected and stored on magnetic tape. The dominant reaction channels populated were the $4n$, $5n$, $6n$, $p4n$, and $\alpha 4n$ channels leading to ^{126}Xe, ^{125}Xe, ^{124}Xe, ^{125}I, and ^{122}Te residual nuclei, respectively. The results from the same experiment on ^{126}Xe [8] and ^{124}Xe [15] are already published.

For the off-line analysis, the calibrated and gain-matched data were sorted into three- and four-dimensional arrays using the software package RADWARE [31]. To determine the multipolarity of γ-ray transitions, two angular distribution matrices were sorted. The first one contained events detected at forward and backward angles (fb), close to average angles of 35° and 145°, repectively, on one axis and those registered in all detectors on the other axis (all). Similarly, the second matrix contained events detected around 90° on one axis (90) and those of all detectors on the other axis. Coincidence gates were set in these matrices on the axis with events detected in all detectors. The intensity ratios $R_\theta = I(\gamma_2^{\rm fb}, \gamma_1^{\rm all})/I(\gamma_2^{90}, \gamma_1^{\rm all})$ were around 0.6 and 1.2 for stretched dipole and stretched quadrupole transitions, respectively.

III. RESULTS AND LEVEL SCHEME

The level scheme of ^{125}I, given in Fig. 1, has been constructed using the observed coincidence relationships between γ-ray transitions and the measured intensities. Spins of the

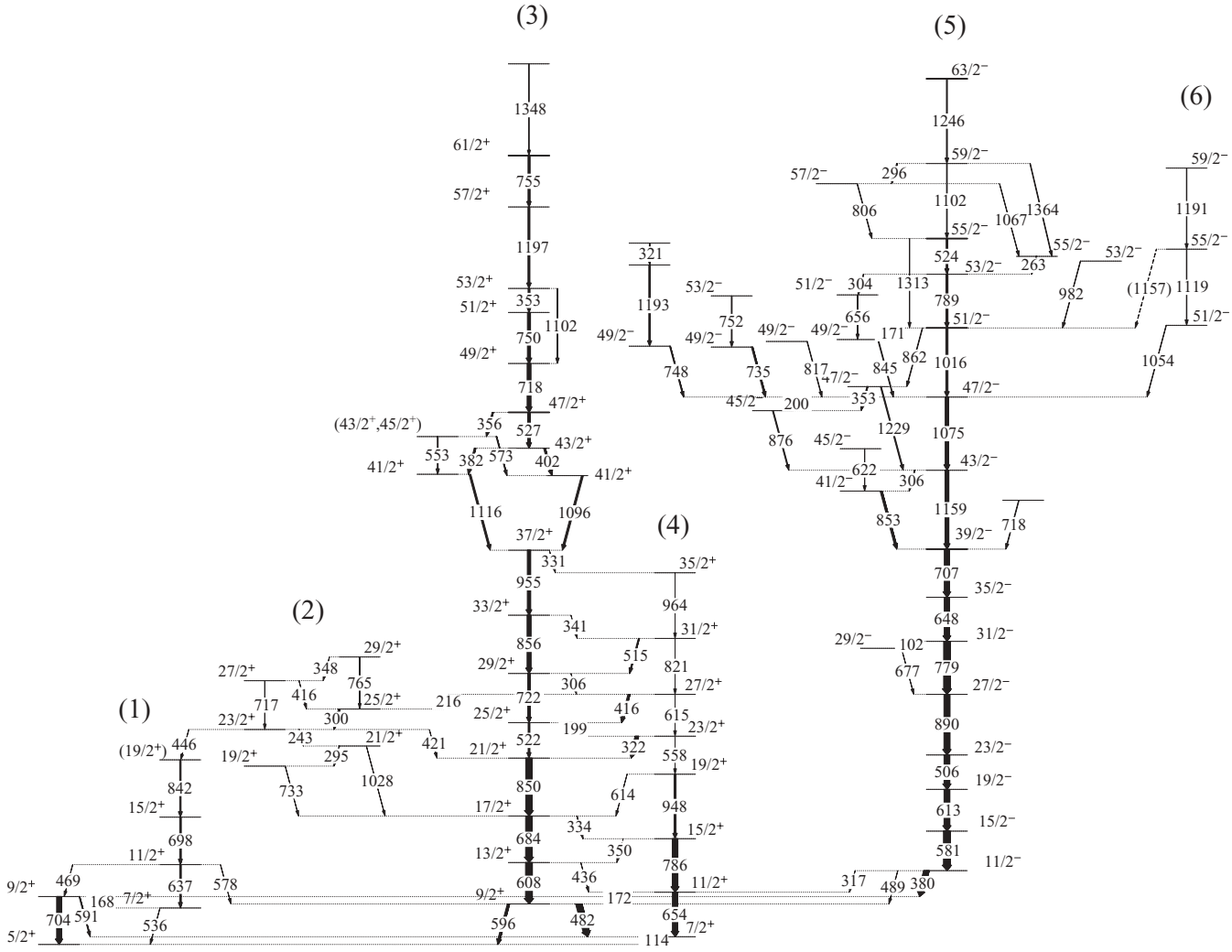

FIG. 1. Partial level scheme of ^{125}I. Note that only the lowest-spin states in the highly deformed band 6 [29] are shown. The noncollective aligned and antialigned states are highlighted by thick lines.

levels have been assigned on the basis of measured angular distribution ratios. In some cases, the presence of crossover and interband transitions helped in assigning spins. The parity of known bands has been adopted from previous work [23,28].

The γ-ray energies, intensities, angular distribution ratios, the adopted multipolarities, level energies, and spin assignments for all transitions observed in ^{125}I are listed in Table I.

A. Positive-parity states

Band 1 was known from previous work up to $I^{\pi} = 19/2^{+}$ [23,27]. In our work, we confirm the transitions of the band and observe a transition of 445.7 keV from the $23/2^{+}$ level of band 2 to the $19/2^{+}$ state of band 1. We could not determine the multipolarity of any of the transitions of band 1 owing to their low intensity. Spin and parity of the levels were adopted from the previous studies.

The sequence of γ-ray transitions with energies of 295.2, 242.6, and 300.5 keV of band 2 were known from the work of Sharma *et al.* [27]. However, only the multipolarity of the 295.2-keV transition was known. We confirm these transitions and extend the sequence by several transitions to higher energies (see Fig. 1). A summed triple-gated γ-ray coincidence spectrum with transitions of band 2 is displayed in Fig. 2.

A transition of 216.3 keV from the $27/2^{+}$ state of band 4 to the $25/2^{+}$ level of band 2 has been observed, independently confirming the placement of band 2 within the level scheme. Band 2 decays to the lower part of band 3 through the 733.0- and 1028.2-keV γ rays. Note that an energy of 736 keV was assigned to the former transition in the work of Sharma *et al.* [23]. The measured angular distribution ratio of 1.15(21) for the 1028.2-keV transition depopulating the 2915.5-keV level agrees well with an $E2$ multipolarity and, hence, $I^{\pi} = 21/2^{+}$ has been assigned to this state. Similarly, a stretched dipole nature could be established for the 242.6-, 295.2-, and 300.5-keV transitions through angular distribution ratio measurements. Two new transitions, most likely of dipole nature, with respective energies of 416.5 and 348.5 keV, have been observed on top of the band. Their placement and ordering are supported by the observed crossover transitions with energies of 765.0 and 717.0 keV.

TABLE I. Energies, intensities, angular distribution ratios, multipolarities, level energies, and spin assignments of γ-ray transitions of ^{125}I.

γ-ray energy E_γ[a] (keV)	Intensity I_γ[b]	Angular distribution ratio R_θ	Multipolarity	Initial level energy E_i (keV)	Assignment		
					J_i^π	→	J_f^π
102.0	24(5)	0.60(4)	$M1$	4453.2	$31/2^-$	→	$29/2^-$
113.5	–	0.66(4)	$M1$	113.5	$7/2^+$	→	$5/2^+$
168.1	–		$M1$	704.1	$9/2^+$	→	$7/2^+$
171.0	38(9)	0.45(2)	$M1$	9057.8	$51/2^-$	→	$49/2^-$
172.1	29(11)		$M1$	767.6	$11/2^+$	→	$9/2^+$
199.4	446(27)	0.61(4)	$M1$	3259.0	$25/2^+$	→	$23/2^+$
199.6	133(13)	0.73(12)	$M1$	8041.7	$47/2^-$	→	$45/2^-$
216.3	93(11)		$M1$	3674.9	$27/2^+$	→	$25/2^+$
242.6	98(11)	0.65(21)	$M1$	3158.1	$23/2^+$	→	$21/2^+$
262.6	100(10)	0.67(5)	$M1$	10109.1	$55/2^-$	→	$53/2^-$
295.2	60(18)		$M1$	2915.5	$21/2^+$	→	$19/2^+$
296.1	114(14)	0.69(3)	$M1$	11472.6	$59/2^-$	→	$57/2^-$
300.5	234(25)	0.59(18)	$M1$	3458.6	$25/2^+$	→	$23/2^+$
303.7[c]	–		$M1$	9846.5	$53/2^-$	→	$51/2^-$
305.8	331(21)	0.58(2)	$M1$	6966.6	$43/2^-$	→	$41/2^-$
306.1	326(28)	0.63(7)	$M1$	3981.0	$29/2^+$	→	$27/2^+$
316.9	24(8)		$E1$	1084.5	$11/2^-$	→	$11/2^+$
321.1	66(10)	0.70(10)	$M1$	10303.5	–	→	–
322.1	520(31)	0.64(2)	$M1$	3059.6	$23/2^+$	→	$21/2^+$
331.4	52(12)	0.69(10)	$M1$	5791.9	$37/2^+$	→	$35/2^+$
333.6	56(16)		$M1$	1887.3	$17/2^+$	→	$15/2^+$
341.1	135(15)	0.57(6)	$M1$	4837.2	$33/2^+$	→	$31/2^+$
348.5	53(11)		$M1$	4223.6	$29/2^+$	→	$27/2^+$
350.3[c]	–		$M1$	1553.7	$15/2^+$	→	$13/2^+$
352.9	246(26)		$M1$	9637.6	$53/2^+$	→	$51/2^+$
353.3	142(15)	0.68(12)	$M1$	8195.4	$47/2^-$	→	$45/2^-$
355.8	188(25)		$M1/E2$	7817.1	$47/2^+$	→	$(43/2^+, 45/2^+)$
380.4	814(45)		$E1$	1084.5	$11/2^-$	→	$9/2^+$
382.2	241(19)	0.59(3)	$M1$	7290.1	$43/2^+$	→	$41/2^+$
402.1	261(20)	0.65(7)	$M1$	7290.1	$43/2^+$	→	$41/2^+$
415.9	316(27)	0.61(6)	$M1$	3674.9	$27/2^+$	→	$25/2^+$
416.5	51(13)		$M1$	3875.1	$27/2^+$	→	$25/2^+$
420.6	90(19)		$M1$	3158.1	$23/2^+$	→	$21/2^+$
435.8	434(41)		$M1$	1203.4	$13/2^+$	→	$11/2^+$
445.7	77(11)		$E2$	3158.1	$23/2^+$	→	$(19/2^+)$
468.9	–		$M1$	1173.0	$11/2^+$	→	$9/2^+$
482.0	921(52)	0.57(3)	$M1$	595.5	$9/2^+$	→	$7/2^+$
489.0	24(8)		$E1$	1084.5	$11/2^-$	→	$9/2^+$
505.6	837(46)	1.23(6)	$E2$	2784.0	$23/2^-$	→	$19/2^-$
515.1	159(15)	0.61(5)	$M1$	4496.1	$31/2^+$	→	$29/2^+$
521.5	231(23)	1.34(17)	$E2$	3259.0	$25/2^+$	→	$21/2^+$
524.0	223(15)	0.76(20)	$M1$	10370.5	$55/2^-$	→	$53/2^-$
527.0	386(25)	1.52(27)	$E2$	7817.1	$47/2^+$	→	$43/2^+$
536.0	–		$M1$	536.0	$7/2^+$	→	$5/2^+$
553.4	105(14)		$M1/E2$	7461.3	$(43/2^+, 45/2^+)$	→	$41/2^+$
558.3	373(34)		$E2$	3059.6	$23/2^+$	→	$19/2^+$
573.3	114(16)		$M1/E2$	7461.3	$(43/2^+, 45/2^+)$	→	$41/2^+$
577.5[c]	–		$M1$	1173.0	$11/2^+$	→	$9/2^+$
580.5	1000(56)		$E2$	1665.0	$15/2^-$	→	$11/2^-$
590.6	117(22)		$M1$	704.1	$9/2^+$	→	$7/2^+$
595.5	347(31)	1.04(8)	$E2$	595.5	$9/2^+$	→	$5/2^+$
607.9	1000(57)		$E2$	1203.4	$13/2^+$	→	$9/2^+$
613.4	843(51)		$E2$	2278.4	$19/2^-$	→	$15/2^-$
613.9[c]	–		$M1$	2501.3	$19/2^+$	→	$17/2^+$
615.3	102(10)		$E2$	3674.9	$27/2^+$	→	$23/2^+$
622.1	50(10)	1.12(14)	$E2$	7282.9	$45/2^-$	→	$41/2^-$

TABLE I. *(Continued.)*

γ-ray energy E_γ[a] (keV)	Intensity I_γ[b]	Angular distribution ratio R_θ	Multipolarity	Initial level energy E_i (keV)	Assignment		
					J_i^π	→	J_f^π
637.0	–		$E2$	1173.0	$11/2^+$	→	$7/2^+$
647.7	779(44)	1.07(4)	$E2$	5100.8	$35/2^-$	→	$31/2^-$
654.1	771(61)		$E2$	767.6	$11/2^+$	→	$7/2^+$
656.0	48(11)	0.74(8)	$M1$	9542.8	$51/2^-$	→	$49/2^-$
676.6	22(4)		$M1$	4351.1	$29/2^-$	→	$27/2^-$
683.9	975(55)	1.05(4)	$E2$	1887.3	$17/2^+$	→	$13/2^+$
697.5	–		$E2$	1870.5	$15/2^+$	→	$11/2^+$
704.1	697(67)		$E2$	704.1	$9/2^+$	→	$5/2^+$
706.9	649(43)	1.14(3)	$E2$	5807.8	$39/2^-$	→	$35/2^-$
717.0[c]	–		$E2$	3875.1	$27/2^+$	→	$23/2^+$
718.0	535(37)	0.56(3)	$M1$	8535.1	$49/2^+$	→	$47/2^+$
718.3	79(12)		–	6526.1	–	→	$39/2^-$
722.0	351(27)	1.21(8)	$E2$	3981.0	$29/2^+$	→	$25/2^+$
733.0	46(17)		$M1$	2620.3	$19/2^+$	→	$17/2^+$
734.6	216(17)	0.77(15)	$M1$	8776.3	$49/2^-$	→	$47/2^-$
747.7	130(20)	0.81(17)	$M1$	8789.4	$49/2^-$	→	$47/2^-$
749.6	451(31)	0.78(7)	$M1$	9284.7	$51/2^+$	→	$49/2^+$
752.0	113(19)	1.08(10)	$E2$	9528.3	$53/2^-$	→	$49/2^-$
754.8	271(23)	1.07(8)	$E2$	11589.4	$61/2^+$	→	$57/2^+$
765.0	49(13)		$E2$	4223.6	$29/2^+$	→	$25/2^+$
778.6	857(48)	1.11(13)	$E2$	4453.2	$31/2^-$	→	$27/2^-$
786.1	817(48)		$E2$	1553.7	$15/2^+$	→	$11/2^+$
788.7	287(21)	0.66(7)	$M1$	9846.5	$53/2^-$	→	$51/2^-$
806.0	66(13)	0.71(10)	$M1$	11176.5	$57/2^-$	→	$55/2^-$
816.9	67(13)	0.72(10)	$M1$	8858.6	$49/2^-$	→	$47/2^-$
821.2	96(13)		$E2$	4496.1	$31/2^+$	→	$27/2^+$
841.9	198(20)		$E2$	2712.4	$(19/2^+)$	→	$15/2^+$
845.2	109(13)	0.52(9)	$M1$	8886.8	$49/2^-$	→	$47/2^-$
850.2	947(59)	1.16(4)	$E2$	2737.5	$21/2^+$	→	$17/2^+$
853.0	301(21)	0.46(7)	$M1$	6660.8	$41/2^-$	→	$39/2^-$
856.2	552(36)	1.19(6)	$E2$	4837.2	$33/2^+$	→	$29/2^+$
862.4	76(12)	1.02(8)	$E2$	9057.8	$51/2^-$	→	$47/2^-$
875.5	138(14)	0.65(7)	$M1$	7842.1	$45/2^-$	→	$43/2^-$
890.4	867(49)	1.22(10)	$E2$	3674.4	$27/2^-$	→	$23/2^-$
947.6	286(19)	0.96(2)	$E2$	2501.3	$19/2^+$	→	$15/2^+$
954.6	479(31)	1.09(6)	$E2$	5791.9	$37/2^+$	→	$33/2^+$
964.4	92(14)	1.17(14)	$E2$	5460.5	$35/2^+$	→	$31/2^+$
981.7	57(12)	0.67(08)	$M1$	10039.5	$53/2^-$	→	$51/2^-$
1016.2	312(22)	1.20(4)	$E2$	9057.8	$51/2^-$	→	$47/2^-$
1028.2	159(31)	1.15(21)	$E2$	2915.5	$21/2^+$	→	$17/2^+$
1054.0	56(11)	1.06(12)	$E2$	9095.7	$51/2^-$	→	$47/2^-$
1067.4	47(10)		$M1$	11176.5	$57/2^-$	→	$55/2^-$
1075.1	507(32)	1.07(3)	$E2$	8041.7	$47/2^-$	→	$43/2^-$
1096.1	279(20)	1.06(7)	$E2$	6888.0	$41/2^+$	→	$37/2^+$
1102.1	102(12)	1.17(10)	$E2$	11472.6	$59/2^-$	→	$55/2^-$
1102.5	105(14)	1.02(10)	$E2$	9637.6	$53/2^+$	→	$49/2^+$
1116.0	264(20)	1.09(9)	$E2$	6907.9	$41/2^+$	→	$37/2^+$
1118.8	64(18)	1.05(10)	$E2$	10214.4	$55/2^-$	→	$51/2^-$
1158.8	559(33)	1.02(3)	$E2$	6966.6	$43/2^-$	→	$39/2^-$
1157.0[c]	–		$E2$	10214.4	$55/2^-$	→	$51/2^-$
1191.4	60(10)	1.41(23)	$E2$	11405.8	$59/2^-$	→	$55/2^-$
1193.0	161(20)		–	9982.4	–	→	$49/2^-$
1197.0	289(23)	1.32(9)	$E2$	10834.6	$57/2^+$	→	$53/2^+$
1228.8	151(18)	0.85(27)	$E2$	8195.4	$47/2^-$	→	$43/2^-$
1245.6	138(22)	1.07(9)	$E2$	12718.2	$63/2^-$	→	$59/2^-$
1312.7	48(15)	1.29(12)	$E2$	10370.5	$55/2^-$	→	$51/2^-$

TABLE I. *(Continued.)*

γ-ray energy E_γ[a] (keV)	Intensity I_γ[b]	Angular distribution ratio R_θ	Multipolarity	Initial level energy E_i (keV)	Assignment		
					J_i^π	→	J_f^π
1348.0	59(13)		–	12937.4	–	→	$61/2^+$
1363.5	84(20)		$E2$	11472.6	$59/2^-$	→	$55/2^-$

[a]Uncertainties are between 0.2 and 0.6 keV depending upon their intensity.
[b]Intensities are normalized to the 580.5- and 607.9-keV transitions, respectively, with $I_\gamma = 1000$.
[c]Measurement of intensity and angular distribution ratio not possible due to presence of γ ray of overlapping energy.

Band 3 (see Fig. 1) was observed previously up to a 3868.2-keV level with a tentative spin assignment of $25/2^+$ [23,27]. We confirm these transitions with the exception of the 1130-keV γ ray and extend the band further up to the $61/2^+$ level. In Fig. 3, a triple-gated coincidence spectrum is displayed where the newly observed transitions of band 3 can be seen. Four γ rays with energies of 521.5, 722.0, 856.2, and 954.6 keV have been placed on top of the $21/2^+$ level, extending band 3 to the $37/2^+$ state. The angular distribution ratios for all four transitions are compatible with a quadrupole nature (see Table I). The levels of band 3 up to the $37/2^+$ state and those of band 4 up to the $35/2^+$ level (see the following) form a coupled band structure.

The level sequence between the $37/2^+$ and $47/2^+$ states of band 3 exhibits an irregular pattern. The $37/2^+$ state is populated by two parallel transitions of 1116.0 and 1096.1 keV. The angular distribution ratios of 1.09(9) and 1.06(7), respectively, for these transitions clearly indicate their quadrupole, probably $E2$, character. Therefore, spin and parity of $41/2^+$ have been assigned to the 6908- and 6888-keV levels. The two $41/2^+$ states are fed by two dipole transitions with energies of 382.2 and 402.1 keV from a $43/2^+$ state. A 527.0-keV γ ray has been observed in coincidence with these four transitions and has been placed above the $43/2^+$ state. The $E2$ character of this 527-keV transition is consistent with the measured value $R_\theta = 1.5(3)$. Another decay path, connecting the $47/2^+$ state at 7817 keV and both $41/2^+$ levels, has been observed through the 355.8-, 553.4-, and 573.3-keV transitions. We could not determine the multipolarity of any of these transitions owing to the presence of intense γ rays with overlapping energies from neighboring nuclei. Hence, spin and parity of $43/2^+$ or $45/2^+$ have been tentatively proposed for the intermediate level.

A cascade of six γ rays with energies of 718.0, 749.6, 352.9, 1197.0, 754.8, and 1348.0 keV has been observed in coincidence with the transitions from the lower part of band 3. We have placed these transitions, ordered according to their intensities, above the $47/2^+$ state. The ratios $R_\theta = 0.56(3)$ and 0.78(7) for the 718.0- and 749.6-keV γ rays, respectively, confirm their dipole nature, whereas the values $R_\theta = 1.32(9)$ and 1.07(8) for the 1197.0- and 754.8-keV transitions, respectively, indicate that they are of $E2$ multipolarity. Furthermore, we have observed a 1102.5-keV transition parallel to the 352.9- and 749.6-keV sequence between the $53/2^+$ and $49/2^+$ states. The spin of the topmost level of band 3 could not be established because of poor statistics of the 1348.0-keV γ ray. We could not place the 1187-, 886-, 882-, and 366-keV γ rays in the present level scheme. These transitions were observed in the sum spectrum produced by gates on γ rays from the lower-energy states of band 3.

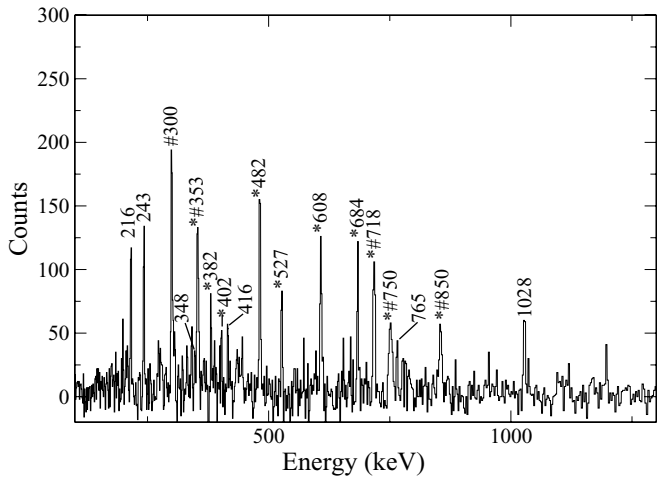

FIG. 2. Summed triple-gated γ-ray coincidence spectrum showing transitions of band 2. The spectrum was created using a list of transitions from the ground band and from band 2. The peaks marked with asterisks belong to band 3; hash-marked peaks are unresolved doublets.

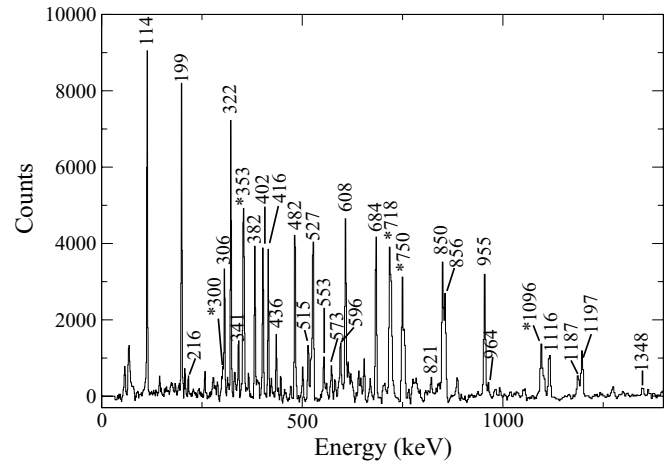

FIG. 3. Summed triple-gated γ-ray coincidence spectrum showing transitions of band 3. The spectrum was created using a list of transitions from band 3 up to the $21/2^+$ level. The peaks marked with asterisks are unresolved doublets.

Band 4 (see Fig. 1) was known up to the $19/2^+$ state from previous studies [23,27]. It was identified as the unfavored signature partner of band 3. We extend band 4 to the $35/2^+$ state by the 558.3-, 615.3-, 821.2-, and 964.4-keV γ rays. In addition, transitions with energies of 322.1, 199.4, 415.9, 306.1, 515.1, 341.1, and 331.4 keV, connecting bands 3 and 4, have been observed. Angular distribution ratios for these transitions establish their dipole character (see Table I).

B. Negative-parity states

Negative-parity states in ^{125}I were previously known up to the $43/2^-$ level [28]. The present experiment confirms the previous results and reveals high-spin transitions up to the $63/2^-$ state. In addition, several decay branches feeding into the yrast sequence at higher spin have been observed. Transitions of 676.6 and 718.3 keV have been placed parallel to the previously known transitions with energies of 778.6 and 1158.8 keV, respectively. A representative triple-gated coincidence spectrum is provided in Fig. 4.

Five γ-ray transitions with energies of 1016.2, 788.7, 524.0, 1102.1, and 1245.6 keV have been placed in cascade above the $47/2^-$ level. Their ordering has been established on the basis of their intensities, determined in spectra gated on low-lying transitions. Several states with the same spin form an irregular structure around spin $49/2^-$. The spin determination of the levels was limited to γ rays with intensities sufficient for a measurement of the angular distribution ratios. In some cases, the presence of more than one decay branch between two levels was helpful in determining the spins of the levels. The angular distribution ratios of the 1016.0-, 1102.1-, and 1245.6-keV γ rays are 1.20(4), 1.17(10), and 1.07(9), respectively, indicating their $E2$ nature. The 788.7- and 524.0-keV γ rays have been assumed to be of $M1$ character following their R_θ values of 0.66(7) and 0.76(20). This assignment is in accordance with the presence of a crossover transition of 1312.7 keV with an angular distribution ratio of $R_\theta = 1.29(12)$. The $59/2^-$ state of band 5 shows decays to the $53/2^-$ and $55/2^-$ levels through three different paths (see Fig. 1). The $\Delta I = 1$ nature of the 806.0-, 296.1-, and 262.6-keV γ rays was established from the respective ratios $R_\theta = 0.71(10)$, 0.69(5), and 0.67(5), which determines the spin of the intermediate states of the decay branches.

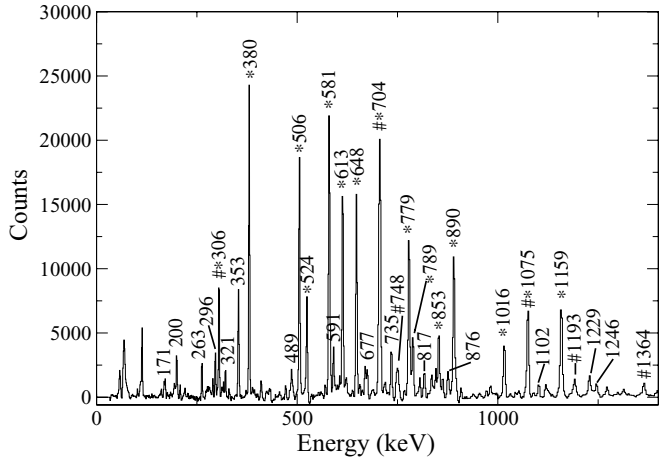

FIG. 4. Summed triple-gated γ-ray coincidence spectrum showing γ rays belonging to negative-parity states. The spectrum was created using a list of transitions from the lower part of band 5. The peaks marked with asterisks belong to yrast states. Hash-marked peaks are unresolved doublets.

IV. DISCUSSION

The low-energy level structure of ^{125}I was interpreted satisfactorily within the framework of the particle-vibrator-coupling model at modest oblate deformation ($\beta_2 = -0.15$) [25–27]. The excited states were explained by coupling an odd proton in the $g_{7/2}$, $d_{5/2}$, or $h_{11/2}$ orbitals to the vibrational states of the neighboring even-even ^{124}Te core. At higher spins, states based on three- and five-quasiparticle excitations become yrast. The aligned angular momenta of bands 2, 3, and 4, displayed in Fig. 5, all exhibit a gain of about $6\hbar$, suggesting that the alignment of $h_{11/2}$ neutrons is involved.

To interpret the high-spin states, calculations within the framework of the CNS formalism [7,32,33] were carried out. The so-called $A = 110$ parameters were used, which are known to give a good description of smooth band termination in the neutron-deficient $Z = 49$–54 nuclei [7]. With the developments described in Ref. [33], absolute energies based on the Lublin-Strasbourg drop model [34] can now be calculated. The orbitals are distinguished according to their N shell. At the deformation of the ground state, one can generally distinguish between orbitals with the main amplitude in different groups of j shells (i.e., in either the high-j intruder shell or distributed over the other j shells within the N shell). For each group of particles in one or several j shells, a division is made into orbitals with signature $\alpha = 1/2$ and $\alpha = -1/2$. Pairing is neglected, which implies that the results are mainly relevant for the description of high-spin states (i.e., for $I > 15$ in this region).

In the following, the new features of the ^{125}I level scheme established in the present work will be summarized. Assignments of configurations for the low-spin states are adopted from previous work. For the higher-spin states, configurations

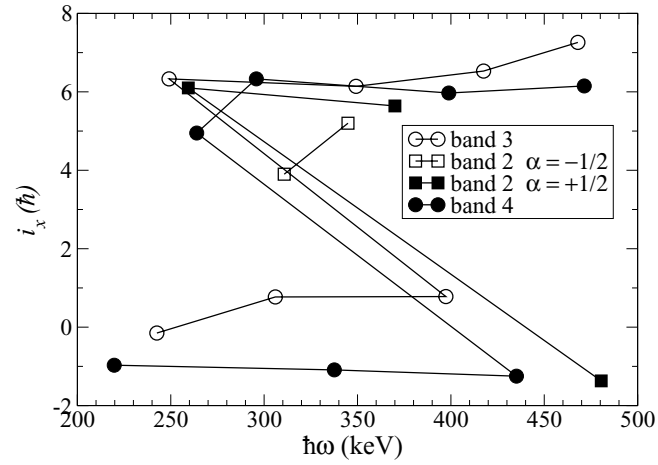

FIG. 5. Aligned angular momenta of bands 2, 3, and 4. A reference core with Harris parameters $J_0 = 20\hbar^2$/MeV and $J_1 = 10\hbar^4$/MeV^3 was used.

are assigned on the basis of systematics of similar structures in neighboring nuclei as well as by comparison with calculations. The structure of the noncollective aligned and antialigned states will be discussed in detail within the framework of the CNS formalism.

A. Low- and medium-spin states

The configurations of bands 1 to 4 are believed to involve positive-parity protons in the $g_{7/2}$ and $d_{5/2}$ orbitals. In this mass region, these orbitals lie close in energy and, hence, strong mixing in the wave functions is expected.

For band 1, which was weakly populated in the present reaction, Sharma *et al.* [23] suggested a $\pi d_{5/2}$ configuration with oblate deformation. A similar band was observed in ^{123}I [35]. In view of these results and the close similarity in the systematics of neighboring odd-A isotopes, this configuration for band 1 is adopted here as well.

Bands 3 and 4 have been explained previously as arising mainly from $\pi g_{7/2}$ configurations, with admixtures of $\pi d_{5/2}$ in the higher-lying states [26]. Later, Sharma *et al.* [23,27] observed interband transitions between the two sequences and interpreted them as $\alpha = +1/2$ and $\alpha = -1/2$ signature partners. Thus, the states up to $21/2^+$ can be associated with the coupling of a proton in the $g_{7/2}$ orbital (with a $d_{5/2}$ admixture) to the 0^+, 2^+, 4^+, 6^+, and 8^+ states of the ^{124}Te core. The irregularities observed above $I^\pi = 19/2^+$ in band 4 and $21/2^+$ in band 3 indicate a change in structure, most likely associated with the breaking of an $h_{11/2}$ neutron pair. A similar change in structure has been observed in the neighboring even-even Te nuclei [36]. Further support for this scenario comes from the energy staggering of bands 3 and 4, plotted in Fig. 6. The large signature splitting observed at low energy suggests the involvement of low-Ω orbitals. The splitting decreases above the $21/2^+$ level, consistent with a three-quasiparticle configuration. The most likely configuration for the states above $21/2^+$ may be $\pi g_{7/2} \otimes \nu h^2_{11/2}$. Above $I^\pi = 37/2^+$, the level scheme shows irregular structures, which are most probably due to further quasiparticle excitations.

Band 2 starts at relatively high spin, $I^\pi = 19/2^+$, and excitation energy, 2620 keV, and is probably associated with a three-quasiparticle excitation (see Fig. 5). Possible three-quasiparticle configurations for this sequence are $\pi g_{7/2} \otimes \nu h^2_{11/2}$, $\pi d_{5/2} \otimes \nu h^2_{11/2}$, and $\pi h_{11/2} \otimes \nu[g_{7/2} h_{11/2}]$. Of these, the latter can be ruled out because band 2 does not decay to band 5, which involves an $h_{11/2}$ proton in its configuration (see the following). It decays preferentially to bands 3 and 4, which are based on a proton $g_{7/2}$ excitation. The 445.7-keV decay from the $23/2^+$ state of band 2 to the $19/2^+$ level of band 1 may result from mixing between the $g_{7/2}$ and $d_{5/2}$ orbitals. Furthermore, the magnitude of the energy staggering for band 2 is similar to that for bands 3 and 4 (see Fig. 6). Thus, the most likely configuration of band 2 is the first of the three configurations mentioned here. It is the same three-quasiparticle configuration as that of bands 3 and 4; however, the bands may correspond to shapes with different triaxiality. A similar pair of bands has been observed in neighboring ^{123}I [37].

$B(M1)/B(E2)$ ratios are sensitive to the configurations involved. These ratios, derived from the $\Delta I = 1/\Delta I = 2$ γ-ray branching ratios for band 2 and bands 3 and 4, are displayed in Fig. 7. Only one data point for band 2 could be obtained owing to the presence of intense γ rays with overlapping energies. The ratios are compared with those calculated for the $\pi g_{7/2}$, $\pi g_{7/2} \otimes \nu h^2_{11/2}$, and $\pi d_{5/2} \otimes \nu h^2_{11/2}$ configurations using the geometrical model of Dönau [38] and Frauendorf [39]. In the calculation, the $E2/M1$ mixing ratios for the dipole transitions have been assumed to be zero. The rotational gyromagnetic factor g_R has been taken as Z/A and the relevant empirical g_k factors for the different single particles have been adopted from Ref. [40]. The quadrupole moment, $Q_0 = 2.03$ b, has been taken from Ref. [37]. As is evident from Fig. 7, the three-quasiparticle structures of band 2 and bands 3 and 4 have very similar $B(M1)/B(E2)$ ratios, which agrees well with the $\pi g_{7/2} \otimes \nu h^2_{11/2}$ configuration. This supports the suggestion that both structures have the same configuration, however, probably with different deformations.

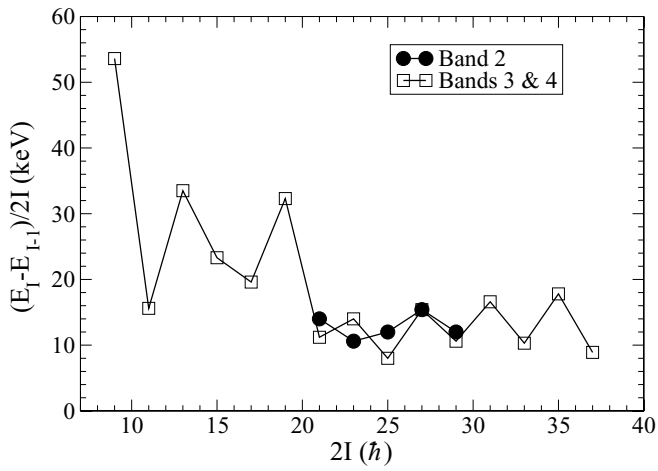

FIG. 6. Energy staggering for band 2 and bands 3 and 4.

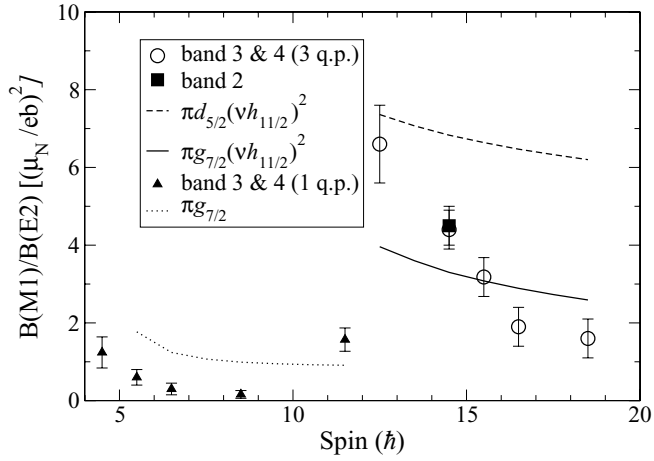

FIG. 7. $B(M1)/B(E2)$ ratios derived from γ-ray branching ratios for one-quasiparticle (triangles) and three-quasiparticle structures (circles) for bands 3 and 4 and for band 2 (square). The calculated values using the geometrical model of Dönau and Frauendorf for different configurations are shown as lines.

A variation of the quadrupole moment within 20% does not change this conclusion.

Band 5 forms the favored negative-parity yrast sequence, as seen in Fig. 1. However, the unfavored signature partner of this band, as reported by Sharma *et al.* [23], was not observed in the present work. Particle-rotor-model calculations [41] support the interpretation of this structure as a decoupled band based on the $11/2^-$ bandhead arising from the proton $h_{11/2}$ orbital with a moderate prolate deformation. The negative-parity states at low energy closely resemble the ground-state band in neighboring even-even ^{124}Te, which has a vibrational nature [36].

B. Aligned and antialigned states

The highest-spin states in valence configurations with six, five, and four $h_{11/2}$ neutrons are formed from the valence particles outside the ^{114}Sn core as

$$\nu(h_{11/2})^6_{18}(s_{1/2}d_{3/2})^2_2, \quad I^\pi_{\max} = 20^+,$$
$$\nu(h_{11/2})^5_{35/2}(s_{1/2}d_{3/2})^3_{3/2}, \quad I^\pi_{\max} = 19^-,$$
$$\nu(h_{11/2})^4_{16}(s_{1/2}d_{3/2})^4_0, \quad I^\pi_{\max} = 16^+.$$

These structures are illustrated in sloping Fermi surface diagrams at their calculated deformation, $\varepsilon_2 \approx 0.12$, in the center panel of Fig. 8. When combined with the favored aligned proton structure (left panel of Fig. 8),

$$\pi(d_{5/2}g_{7/2})^2_6(h_{11/2})^1_{11/2}, \quad I^\pi_{\max} = 23/2^-,$$

they give rise to low-lying states with $I^\pi = 63/2^-$, $61/2^+$, and $55/2^-$, respectively. The calculated energies of the corresponding configurations are given up to these fully aligned states in the center panel of Fig. 9. They are compared with the observed states given in the upper panel. The difference between experiment and calculations is displayed in the lower panel. Note that the fully aligned states are calculated to lie low in energy and they all have a correspondence with observed levels. The fully aligned $55/2^-$ state of ^{121}I [14] is also of the type $\pi h_{11/2}\nu(h_{11/2})^4$, with four $(d_{3/2}s_{1/2})$ particles coupled to $I = 0$ added in the $55/2^-$ state of ^{125}I.

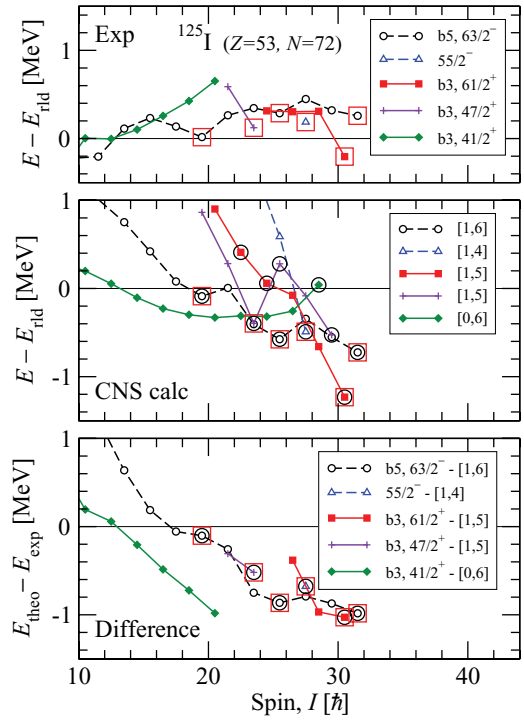

FIG. 9. (Color online) Energies, relative to a rotating-liquid-drop energy, for low-lying observed (upper panel) and calculated (center panel) valence-space states for ^{125}I as well as the difference between experiment and calculations (lower panel). The observed states belonging to bands 3 (b3) and 5 (b5) are labeled by the highest-spin states in the different sequences with fixed signature. In addition, the low-lying $55/2^-$ state is included. The calculated configurations are labeled by the number of $h_{11/2}$ protons and neutrons, respectively. Aligned states are encircled; open squares indicate the observed and corresponding calculated states, which appear especially low in energy.

In Fig. 9, a fourth configuration is presented, which is of the type $\nu(h_{11/2})^5$, but with an unfavored signature for the $h_{11/2}$ neutrons in the $I_{\max}$ state. Thus, it is less favored in energy at termination and seems to have no experimental counterpart. Instead, it appears relatively low in energy with

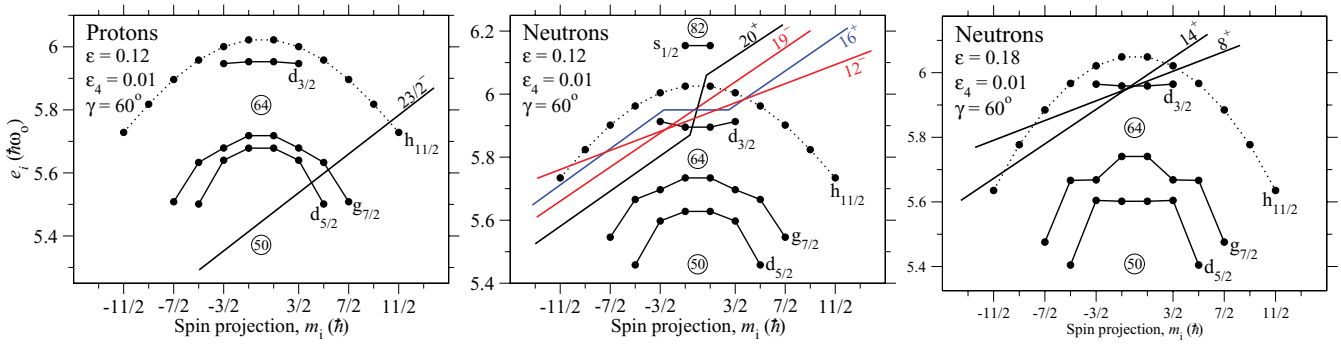

FIG. 8. (Color online) The favored aligned states for the $Z = 53$ configuration with one $h_{11/2}$ proton and the $N = 71$ configurations with six $h_{11/2}$ neutrons, all fully aligned (20^+), and with one (14^+) and two (8^+) antialigned, with five $h_{11/2}$ neutrons fully aligned (19^-) and one antialigned (12^-), and, finally, with four fully aligned $h_{11/2}$ neutrons (16^+). In the latter case the remaining four neutrons fill the $d_{3/2}$ subshell and, thus, do not contribute to the spin. The different structures are drawn close to their equilibrium deformations, which can be read from Fig. 10.

one spin vector antialigned (see the following). Note also that, in Fig. 8, the low-lying $\nu(h_{11/2})^5$ 19^- state is represented by a straight-line Fermi surface, in contrast to the $\nu(h_{11/2})^6$ 20^+ state and the $\nu(h_{11/2})^4$ 16^+ level. This is consistent with the fact that the aligned $61/2^+$ state is observed and calculated to be more favored in energy than the $63/2^-$ and the $55/2^-$ states (see Fig. 9).

Going to somewhat lower spin values, we calculate low-energy states for the $\nu(h_{11/2})^6$ configuration with one or two $h_{11/2}$ neutrons antialigned and with one such neutron antialigned in the $\nu(h_{11/2})^5$ configuration. With one antialigned neutron, the approximate deformation is $\varepsilon_2 = 0.15$, whereas it is $\varepsilon_2 = 0.18$ with two neutrons antialigned. As illustrated in Fig. 8, these three states can be represented by straight-line Fermi surfaces at their approximate deformation.

When the structures with six aligned neutrons, illustrated in Fig. 8, are combined with the favored $\pi h_{11/2}$ proton structure, they give rise to the low-lying calculated states highlighted by squares in the middle panel of Fig. 9. The observed states that can be assigned to them are highlighted in the same way in the upper panel. It is gratifying that an interpretation has been found for all the states observed at relatively low energy. One could even imagine that the low-lying $I^\pi = 23/2^-$ state can be understood as being built from the fully aligned proton structure illustrated in Fig. 8, but with no spin contribution from the neutrons. However, this state is not obtained as an oblate ($\gamma = 60^\circ$) total-energy minimum in the CNS calculations.

For the favored negative-parity configuration, one can define a "rotational" band, as drawn in the three panels of Fig. 9. The corresponding energy surfaces for this fixed configuration are given in Fig. 10. Starting at the low-spin end, one notes a small collectivity for $I^\pi = 35/2^-$ ($\gamma \approx 40^\circ$). A noncollective minimum appears at $\gamma = 60^\circ$ for $I^\pi = 39/2^-$. This is the state with two antialigned neutrons discussed earlier. The next aligned state is observed at $I^\pi = 51/2^-$ with one antialigned neutron, where the corresponding minimum is seen already in the $I^\pi = 39/2^-$ surface at $\gamma \approx 25^\circ$. It migrates toward lower collectivity with increasing spin, with $\gamma \approx 30^\circ$ at $I^\pi = 43/2^-$ and $\gamma \approx 45^\circ$ for $I^\pi = 47/2^-$. A similar trend is observed in the $I^\pi = 51/2^- - 63/2^-$ range for the sequence terminating in the fully aligned $I^\pi = 63/2^-$ state.

The trend toward smaller deformation with increasing spin seen in the energy surfaces can be understood from simple considerations. The orbitals with a high value of m_i (corresponding to Ω in the Nilsson labeling) rotate around the equator and strongly polarize the nucleus toward oblate deformation. There is only one $m_i = 11/2$ orbital in the fully aligned $I^\pi = 63/2^-$ state, whereas there is also one $m_i = -11/2$ orbital involved in the $I^\pi = 51/2^-$ state and both $m_i = \pm 11/2$ and $m_i = \pm 9/2$ orbitals are occupied in the $I^\pi = 39/2^-$ state.

The difference between experiment and calculations seen in the lower panel of Fig. 9 is very much as expected. At high spin, the calculated energies are approximately 1 MeV too low, a value in the same range as observed for terminating bands and terminating states in other mass regions at high spin [33], where pairing can be neglected. With decreasing spin, pairing starts to become important, consistent with the trend that the

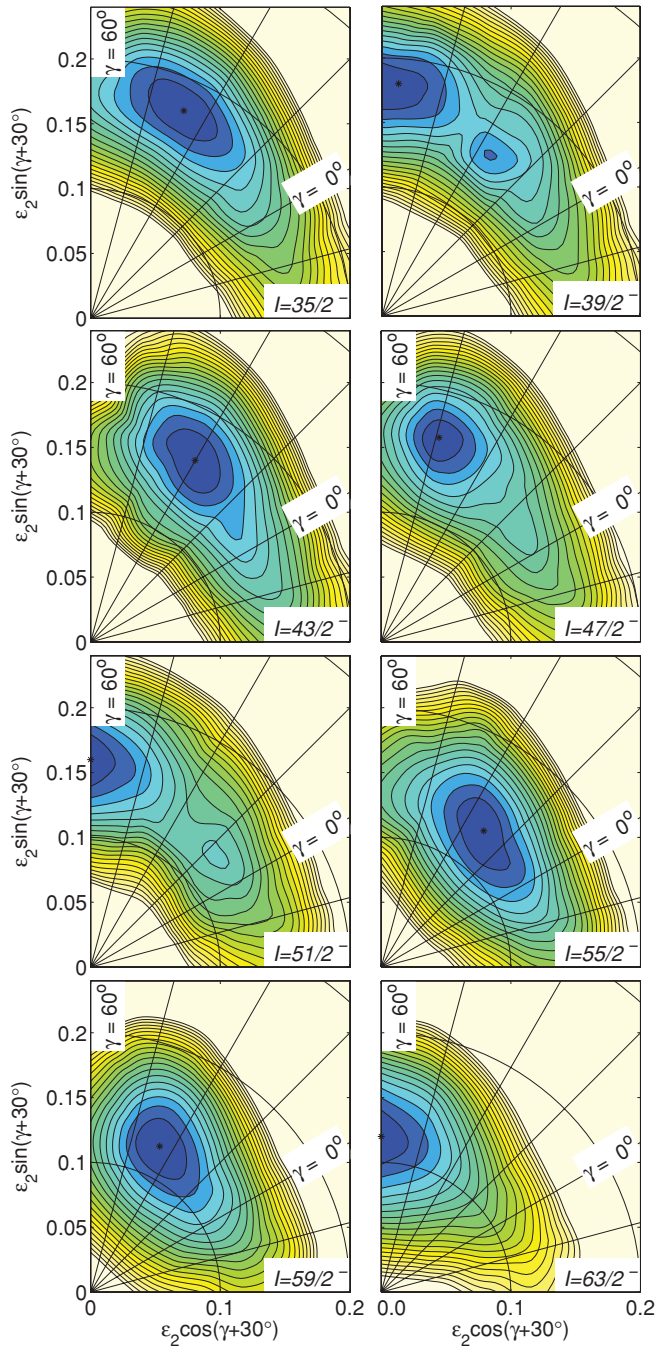

FIG. 10. (Color online) Calculated total energy surfaces for ^{125}I in the spin range $I = 35/2$–$63/2$ of the $\pi h_{11/2}\nu(h_{11/2})^6$ configuration, which is assigned to the observed negative-parity yrast states (band 5). The contour line separation is 0.1 MeV.

observed states appear lower in energy compared with the calculations. In Fig. 9, the configuration with all protons in the $d_{5/2}g_{7/2}$ orbitals is also given. It is naturally assigned to the observed low-spin, positive-parity yrast band. The difference between experiment and calculation indicates a trend with spin similar to that for the other states, but it is somewhat smaller, suggesting that the relative energy between the proton $d_{5/2}g_{7/2}$ subshells and the $h_{11/2}$ subshell is not optimal in the calculations.

Even though the deformation for these fully aligned states is relatively small, it is crucial for the general correspondence between observed and calculated energies seen in Fig. 9. At the state with maximum spin for the structure in Fig. 10, the energy gain from deformation is approximately 2.5 MeV. With increasing deformation for decreasing spin, the energy gain becomes 4.5 and 6 MeV for $I^{\pi} = 51/2^{-}$ and $39/2^{-}$, respectively.

V. SUMMARY

A detailed level scheme, up to the maximum spin available within the valence space for both parities, was established for ^{125}I. In general, with an increasing number of particles outside a core, collective features become more dominant and it is more difficult to identify the maximum-spin states that can be formed from the valence particles outside the ^{114}Sn core. ^{125}I is the heaviest nucleus outside this core where these states have been observed and it exhibits the most complete set of such states among all nuclei in this region. Relative to a rotating liquid drop, six states appear as especially favored in energy, and there exists a one-to-one correspondence with the six noncollective states calculated to lie lowest in energy within the framework of the CNS formalism. In these states, the angular momenta of all eleven valence particles are quantized along a common axis and most of the spin vectors point in the same direction. However, it is of particular interest that in one of the states two of the spin vectors point in the opposite direction; they are antialigned. This is, to our knowledge, the first observation of a state with such a structure. Furthermore, it is also interesting to note that, in the partly irregular level scheme, several structures evolve smoothly from triaxial to oblate shapes, associated with the noncollective aligned states.

ACKNOWLEDGMENTS

Purnima Singh acknowledges financial assistance from the Department of Science and Technology (DST), India. Somnath Nag acknowledges a support from CSIR (India) under Contract No. 09/081(0704)/2009-EMR-I. This work was supported by the DST, India, under Project No. SR/S2/HEP-09/2005, by the Swedish Science Research Council, by the German BMBF under Contract No. 06 BN 109, by the Danish FNU Council for Natural Sciences, and by the US Department of Energy, Office of Nuclear Physics, under Contract Nos. DE-AC02-06CH11357 and DE-AC03-76SF00098.

[1] C.-B. Moon, J. Korean Phys. Soc. **45**, 859 (2004).
[2] C.-B. Moon, and J. U. Kwon, J. Korean Phys. Soc. **32**, 666 (1998).
[3] K. Starosta *et al.*, Phys. Rev. C **64**, 014304 (2001).
[4] M. P. Waring *et al.*, Phys. Rev. C **51**, 2427 (1995).
[5] E. S. Paul, H. R. Andrews, V. P. Janzen, D. C. Radford, D. Ward, T. E. Drake, J. DeGraaf, S. Pilotte, and I. Ragnarsson, Phys. Rev. C **50**, 741 (1994).
[6] E. S. Paul *et al.*, Phys. Rev. C **59**, 1984 (1999).
[7] A. V. Afanasjev, D. B. Fossan, G. J. Lane, and I. Ragnarsson, Phys. Rep. **322**, 1 (1999).
[8] C. Ronn Hansen *et al.*, Phys. Rev. C **76**, 034311 (2007).
[9] A. Al Khatib *et al.*, Phys. Rev. C **74**, 014305 (2006).
[10] I. Ragnarsson, Z. Xing, T. Bengtsson, and M. A. Riley, Phys. Scr. **34**, 651 (1986).
[11] A. K. Singh *et al.*, Phys. Rev. C **70**, 034315 (2004).
[12] A. O. Evans *et al.*, Phys. Rev. Lett. **92**, 252502 (2004).
[13] E. S. Paul *et al.*, Phys. Rev. Lett. **98**, 012501 (2007).
[14] E. S. Paul, J. Simpson, S. Araddad, C. W. Beausang, M. A. Bentley, M. J. Joyce, and J. F. Sharpey-Schafer, J. Phys. G **19**, 913 (1993).
[15] A. Al Khatib *et al.*, Eur. Phys. J. A **36**, 21 (2008).
[16] J. Singh, H. Kaur, A. Sharma, J. Goswamy, D. Mehta, N. Singh, P. N. Trehan, E. S. Paul, and R. K. Bhowmik, Z. Phys. A **356**, 125 (1996).
[17] H. Timmers, J. Simpson, M. A. Riley, T. Bengtsson, M. A. Bentley, F. Hanna, S. M. Mullins, J. F. Sharpey Schafer, and R. Wyss, J. Phys. G **20**, 287 (1994).
[18] J. Simpson *et al.*, Phys. Lett. B **327**, 187 (1994).
[19] A. O. Evans *et al.*, Phys. Rev. C **73**, 064303 (2006).
[20] E. S. Paul *et al.*, Phys. Rev. C **79**, 044324 (2009).
[21] J. S. Geiger, Phys. Rev. **158**, 1094 (1967).
[22] J. Ludziejewaki, J. Kownacki, W. Klamra, J. Chwaszczewaka, and W. Przybski, Acta Phys. Pol. **36**, 939 (1969).
[23] H. Sharma, B. Sethi, R. Goswami, P. Banerjee, R. K. Bhandari, and J. Singh, Phys. Rev. C **59**, 2446 (1999).
[24] J. R. Lien, J. Gard, C. Lunde Nilsen, G. Lovhoiden, and P. B. Vold, Nucl. Phys. A **281**, 443 (1977).
[25] U. Hagemann, H.-J. Keller, and H.-F. Brinckmann, Nucl. Phys. A **289**, 292 (1977).
[26] L. G. Kostova, W. Andrejtscheff, L. K. Kostov, F. Dönau, L. Kaubler, H. Prade, and H. Rotter, Nucl. Phys. A **485**, 31 (1988).
[27] H. Sharma, B. Sethi, P. Banerjee, R. Goswami, R. K. Bhandari, and J. Singh, Phys. Rev. C **63**, 014313 (2000).
[28] C.-B. Moon and T. Komatsubara, J. Korean Phys. Soc. **45**, L791 (2004).
[29] P. Singh *et al.* (to be published).
[30] I. Y. Lee, Nucl. Phys. A **520**, 641 (1990).
[31] D. C. Radford, Nucl. Instrum. Methods A **361**, 297 (1995).
[32] T. Bengtsson and I. Ragnarsson, Nucl. Phys. A **436**, 14 (1985).
[33] B. G. Carlsson and I. Ragnarsson, Phys. Rev. C **74**, 011302(R) (2006).
[34] K. Pomorski and J. Dudek, Phys. Rev. C **67**, 044316 (2003).
[35] S.-Y. Wang *et al.*, J. Phys. G **32**, 283 (2006).
[36] N. Warr, S. Drissi, P. E. Garrett, J. Jolie, J. Kern, H. Lehmann, S. J. Mannanal, and J.-P. Vorlet, Nucl. Phys. A **636**, 379 (1998).
[37] Y.-X. Zhao, T. Komatsubara, Y.-J. Ma, Y.-H. Zhang, S.-Y. Wang, Y.-Z. Liu, and K. Furuno, Chin. Phys. Lett. **26**, 082301 (2009).
[38] F. Dönau, Nucl. Phys. A **471**, 469 (1987).
[39] S. Frauendorf, Phys. Lett. B **100**, 219 (1981).
[40] D. Ward *et al.*, Nucl. Phys. A **529**, 315 (1991).
[41] H. Sharma, B. Sethi, P. Banerjee, R. Goswami, R. K. Bhandari, and J. Singh, Pramana J. Phys. **57**, 171 (2001).